Assessment of Mass Movements and Critical Phreatic Levels in Soil Slopes

D. Ravichandran[1], E. Nishok Kumar[1], R. Ramkrishnan[1(✉)], Karthik Viswanathan[2], S. Sandeep[1], and K. Manasa[1]

[1] Department of Civil Engineering, Amrita School of Engineering, Amrita Vishwa Vidyapeetham, Coimbatore, India
r_ramkrishnan@cb.amrita.edu

[2] Department of Civil and Environmental Engineering, University of California at Berkeley, Berkeley, CA, USA

Abstract. Tectonic movements and vibrations of the earth cannot be controlled, which causes devastating natural hazards like landslides and earthquakes which have accounted for many lives in the previous years. The major reasons for landslides are heavy rainfall, liquefaction, rise in pore water pressure, floods, etc. This experimental study focuses on identifying the Critical Phreatic Level (CPL) of different soil types for different slope geometries. Different soil types were modeled in a tank of dimensions 2.30 × 1.00 × 1.25 m to simulate the natural field conditions like field density, ground water flow and slope angle in the laboratory with scaled down slopes of specific angles, based on the natural angle of repose of the soil. Density closely resembling the natural field density was obtained by air pluviation and a constant water inflow from an adjacent chamber was provided to simulate groundwater flow. The slope geometry was modeled, initial conditions were set and the phreatic level in the slope was continuously monitored until the slope fails with considerable slope displacement. The soil properties such as permeability, bulk unit weight, specific gravity and angle of repose obtained from laboratory tests were used as input parameters to model the slopes in PLAXIS 2D. The displacement values obtained from the software were compared with the displacement values obtained from the experiment, and were found to be similar, thereby validating the results.

1 Introduction

Slope of a soil mass is the gradient or angle of inclination of the soil surface from the horizontal, with one end at a higher level and another at a lower level, also called rising or falling of the earth surface. Formation of these sloped surfaces gives rise to different topographical features on the earth surface, which is either natural or man-made formations with varying slope geometries. These slopes collapse when adverse conditions act upon it. Stability of the soil is its potential to withstand and restrict movement. Under equilibrium conditions the soil slope is acted upon by driving forces and resisting forces, where the driving force is the action of gravity and seepage forces if any, which is resisted by the shear strength of the soil. Soil stability can be defined as the balance of Shear Stress and Shear Strength of the soil, beyond which it fails. Soil

S. Wang et al. (eds.), *New Solutions for Challenges in Applications of New Materials and Geotechnical Issues*, Sustainable Civil Infrastructures,
https://doi.org/10.1007/978-3-319-95744-9_13

failure is defined as the movement of the soil, which is classified into (i) falls (ii) slides and (iii) flows. This phenomenon is influenced by rainfall (Kim et al. 2004; Rahardjo et al. 2005), earthquake (Bray and Travasarou 2007; Hack et al. 2007), pore water pressure (Rinaldi et al. 2004; Smethurst et al. 2006), seepage (Ng and Shi 1998) and surcharge loading (Zhu et al. 2014). Main causes of slope failures are rainfall (Rahimi et al. 2011), Earthquakes (Wilson and Keefer 1984), Seepage (Gasmo et al. 2000), Surcharge load (Sazzad and Haque 2014) and Erosion (Vandamme and Zou 2013). It is vital to understand the characteristics and behavior of soil in a sloped region. Analysis on soil slopes are therefore done to:

- Understand the formation and development of different failures of soil slope and the processes which are responsible for it (Simon et al. 1990),
- Study and monitor the stability of slopes along different scales of time under various conditions,
- Study the soil failure mechanism, type and the environmental factors responsible for the failure,
- Predict the possibility of slope failure for both natural and engineered slopes (Chen and Lee 2003; Saygili and Rathje 2008).

Various analyses are repeatedly performed in order to understand the functional behavior of soil slopes. The prevailing site conditions and the potential mode of failure are considered to be the main factors to be analyzed. The objective of this study is to perform a slope stability analysis on a laboratory scale soil. Natural slopes of varying geometries are scaled down and modeled in a tank of dimensions 2.30 × 1.00 1.25 m. Seepage pressure is induced in the soil mass by promoting a constant inflow rate from an adjacent chamber (Ramkrishnan et al. 2017). The Critical Phreatic Level (the top flow line of a soil mass below which seepage takes place at which the soil fails) for different slope geometries and soil types are found. The experimental results, mainly the CPL for all slope geometries, were analytically modeled using PLAXIS to validate the displacement values obtained from the experimental analysis.

2 Literature Review

Slope failure occurs when the downward movement of soil particles due to gravity and shear stresses exceeds the ultimate shear strength of the soil. The factors that tend to increase the shear stresses or decrease the shear strength increase the chances of failure of a slope. The predominant causes for slope failure are gravity driven groundwater flow, soil topography, effective stresses (Iverson and Reid 1992) etc. Soil topography influences the gravity-driven groundwater flow and the consequent distribution of effective stress, which in turn influences the potential for slope failure. Stability of the slope also depends up on the permeability of the soil as found by Pradel and Raad (1993). Results have shown that reduction in permeability increases the probability of slope saturation, creating the potential for slope failure to occur. Seepage erosion causes liquefaction and rapid slope failures (Crosta and Prisco 1999). The shear strength of the soil can be influenced by transient seepage as stated by Ng and Shi (1998). They concluded that increasing ground water levels result in the decrease of

shear strength. It has been observed that groundwater levels rise due to rainfall and antecedent rainfalls have significant influence on the stability of the slope. The effect of transient seepage in an unsaturated soil slope increases the moisture content and soil permeability leading to slope failure (Lam et al. 1987). Soil-water characteristics are strongly dependent on the confining stress which also plays a major role in slope failure (Ng and Pang 2000).

The relative density of the soil sample depends on drop height, particle size of the soil, impact energy, and the impact velocity (Vaid and Negussey 1984). Pluviation can either be air pluviation or water pluviation (Vaid 1984). The relative density achieved through air pluviation depends on the drop height, uniformity of the sand rain, deposition intensity and the average size of the particle (Kolbuszewski 1948; Kolbuszewski and Jones 1961; Butterfield and Andrawes 1970). This method is widely adopted for preparation of large, uniform and repeated soil sample which are not highly cohesive in nature (Dave and Dasaka 2012). Theoretical study by Vaid and Negussey (1988) shows that impact velocity increases non-linearly with height of fall and with increase in particle size. Also, the impact energy increases with increase in height of fall (Kildalen and Stenhamar 1977). Maintaining a constant height of fall and adjusting deposition index while pluviation will be more appropriate for large scale projects (Drnevich et al. 1987; Saussus and Frost 2000; Dupla et al. 2004; Zhao et al. 2006).

The analysis of stability and deformation in geotechnical engineering projects has been made easy after development of a finite element package, PLAXIS 2D. PLAXIS can be used in various areas such as, simulation of foundation excavation and support (Wang et al. 2007), analysis of soil-structure interaction (Viggiani and Tamagnini 2000), slope stability analysis (Hammouri et al. 2008; Alamshahi and Hataf 2009), etc. Evaluation of stability of slopes utilizes stress strain relationships which can be incorporated using PLAXIS as stated by Aryal (2006). An accurate analysis of a slope stability problem and the associated failure mechanism needs to consider the evolving strains and path dependency by means of a constitutive model (Laouafa and Darve 2002). Another approach of soil modeling includes probabilistic modeling of soil profiles which provides quantified information gathered during site investigation and testing, subsurface conditions at a site and provides the basis for predicting performance (Vanmarcke 1977).

3 Materials and Methodology

3.1 Materials

Soil

Three different types of soil found in and around Coimbatore region, Tamil Nadu, India were used for this analysis. Sieve analysis was performed to determine the grain size distribution of the 3 soil types (Fig. 1) and soil sieved through 10 mm sieve (according to IS classification) was used for modeling the slope. Soil 1 was collected from Ettimadai, Coimbatore and Soil 2 and Soil 3 were collected from different sites near

Kanuvai, Coimbatore, Tamil Nadu. The three different types of soil were tested for their basic properties like permeability, shear parameters, particle size, void ratio, specific gravity, maximum dry density, optimum moisture content, etc., and are tabulated in Table 1.

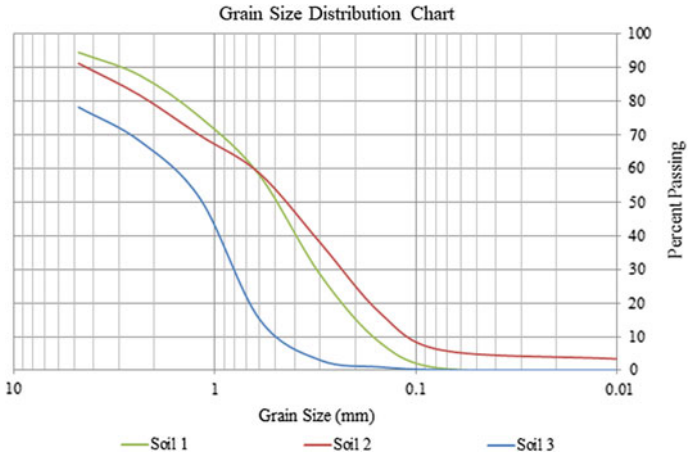

Fig. 1. Grain size distribution for the 3 soils

Table 1. Laboratory experiment results

Parameter	Soil 1	Soil 2	Soil 3
k (m/min)	$8.80e^{-4}$	$3.00e^{-4}$	$4.36e^{-4}$
γ_b (kN/m^3)	23.2	23.6	22.8
G	2.63	2.66	2.42
Φ (degrees)	30.5	41.3	28.9
OMC (%)	11.0	9.00	7.00
C_u	3.22	6.85	3.04
C_c	0.200	0.054	0.151
W_L	14.1	17.5	11.8
W_P	0.00	13.4	18.7
I_P	14.1	6.94	4.05
IS soil classification	SP	SW	SW

3.2 Geotextile

Geotextiles are permeable fabrics made from polypropylene or polyester which, when used in association with soil, can separate, filter, reinforce, protect, or drain. The non-woven geotextile used in this study is shown in Fig. 2 and its properties as provided by the manufacturer are given in Table 2.

Fig. 2. Non-woven geotextile

Table 2. Properties of geotextile

Properties	Standard	200 gsm
Mechanical properties		
Tensile strength	ASTM D 4595	8 kN/m
Elongation	ASTM D 4595	>50%
Physical properties		
Mass/unit area	ASTM D 5261	200 g/m^2
Thickness	ASTM D 5199	1.5 mm
Hydraulic properties		
Flow water head- 5 cm head	ASTM D 4491	50 l/m^2/s
AOS	ASTM D 4751	80 µm

3.3 Tank

A tank with dimensions 2.30 m × 1.00 m × 1.25 m was fabricated using MS metal sheets. One side was provided with windows made of glass, to monitor the slope movement and water level, as shown in Figs. 3 and 4 respectively. The tank was split into two compartments, of length 2.0 m and 0.3 m respectively, using a perforated metal sheet. The perforated sheet was covered with a Non-Woven geotextile material to prevent the movement of sand from one side to the other, but allowing easy movement of water. The larger compartment was used to construct the slope model while the smaller chamber was used as a water tank. This smaller portion was provided with ball valves to regulate the water level in the chamber. The inner surface of the tank was kept smooth to reduce any friction between the tank and the soil, and to ensure its uniform movement within. A graduated scale was fixed on the glass to give an accurate measurement of the water level in the chamber. Grids were drawn inside the tank and on the glass to help in laying the slope accurately and to monitor the slope.

Fig. 3. Tank setup

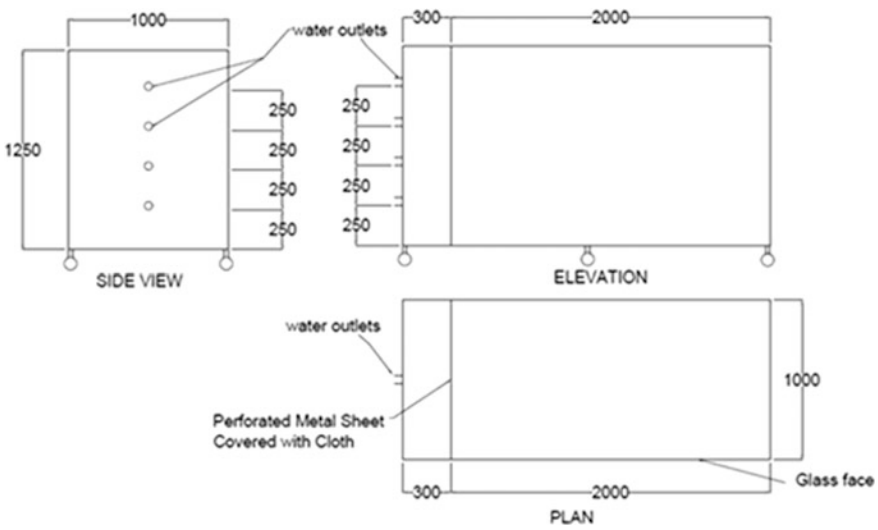

Fig. 4. Tank dimension

3.4 Pluviation Setup

An air pluviation setup, which consists of a pulley system and a pluviation bucket as shown in Fig. 5 was used to model the slopes. The pulley system was designed such that it could be moved throughout the length and breadth of the tank.

3.5 Slope Geometries

A pilot test was conducted to determine the maximum slope angle that could be achieved by air pluviation. The slope was created with a crest height of 0.75 m and a toe height of 0.2 m. The width of the horizontal portion of the crest was altered according to the slope geometry modeled. To get comparable results, the slope angles

Fig. 5. Pluviation setup

chosen were 28°, 30° and 33°. For Soil - 1, the experiment was performed for angles of 28°, 30° and 33°. For Soil - 2 and Soil - 3 the experiments were performed for 28° and 30°. The slope geometries and its dimensions (mm) are shown in Fig. 6 and Table 3 respectively.

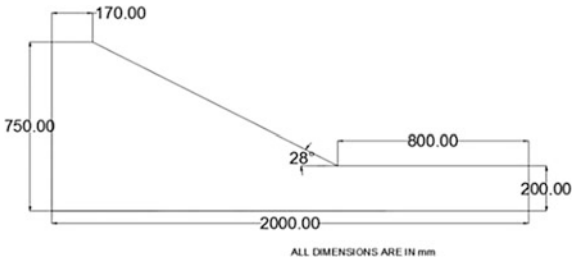

Fig. 6. 28° slope

Table 3. Slope dimensions

Length (mm)			
Slope angle	Crest	Slope	Toe
28°	170	1030	800
30°	250	950	800
33°	353	847	800

3.6 Digital Moisture Sensor (DMS)

The Soil Moisture Sensor, shown in Fig. 7, measures the volumetric water content in the soil. The two probes of the sensor act as a variable resistor – more water in the soil results in better conductivity, lower resistance and higher output voltage. The analog reading varies depending on the voltage used as well as the resolution of the Analogue to Digital Converter (ADC) pins.

Fig. 7. Digital moisture sensors (DMS)

3.7 Sensor Monitoring Setup

A sensor monitoring setup was installed to monitor the fluctuations in the water level of the soil slope. The position of sensor placement in the soil slope was maintained constant for all slope angles. The sensors were placed at an interval of 20 cm along the length of the tank and 5 cm along the height of the tank. Digital Moisture Sensors as mentioned above were used. The leads were placed in the soil at the abovementioned locations, of which the conductivity increases when water reaches the sensor, making the LED glow in the potentiometer. The indication of LED represents that water has reached the sensor position. A sensor monitoring panel was setup outside the tank to continuously monitor the water flow in real-time, as shown in Fig. 9. A representative sensor placement for the 28° slope geometry is shown in Fig. 8.

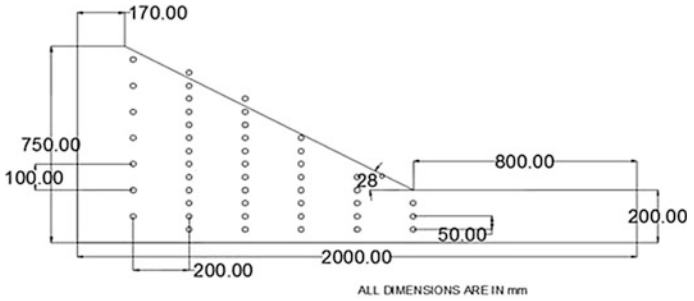

Fig. 8. 28° sensor setup

3.8 Experimental Procedure

The sieved soil sample was poured into the pluviation bucket which was tied to a pulley setup. The height of fall for each soil to achieve the maximum dry density was found by measuring the densities at different fall height. By the to and fro motion of the bucket, soil could flow uniformly through a funnel attached at the bottom. Soil was continuously filled for the first 5 cm and then sensors were placed with an equal interval of 20 cm and 5 cm along length and height of the tank respectively. The process was continued and soil was pluviated to a height of 75 cm at the crest, 20 cm at

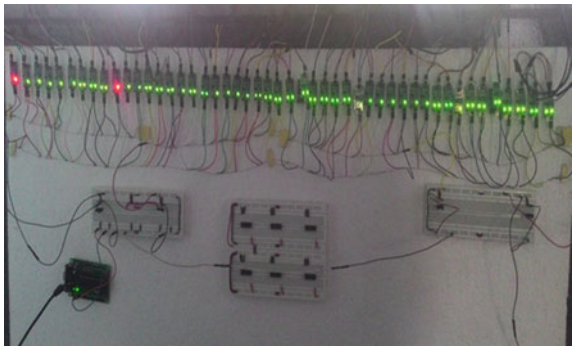

Fig. 9. Sensor monitoring panel

the toe and a length covering 2 m with required slope angle. Dial gauges were fixed at the toe and face of the soil slope to monitor any slope movement. After setting up the model, water with a constant inflow discharge of 2.2 L per minute was induced and maintained throughout the experiment, to simulate a natural groundwater flow condition (Ramkrishnan et al. 2017). Position of the phreatic level and the dial gauge readings were noted for every five minute interval. The experiment continued until the dial gauges showed considerable displacement, indicating ample slope movement or visible slope failure. Outflow discharges were also monitored to ensure steady state flow.

3.9 Numerical Modeling

Numerical studies for the verification of test models were conducted using Finite Element Method (FEM) tools. The plane strain finite element analysis was carried out using PLAXIS 2D software. In this study, the soil was modeled using the Mohr-Coulomb model, which involves five parameters, namely Young's modulus (E), Poisson's ratio (μ), Unit weights, Cohesion(c), and Angle of internal friction (Φ). Finite element analyses were carried out by applying vertical predefined displacements and zero horizontal displacements to the nodes at the top of the soil profile. The specified displacements were applied in equal increments of 250 steps. The soil parameters adopted in all the finite element analyses for the modeled soil slope were tabulated in Table 4. The homogeneous soil slopes of 28º and 30º with induced ground water table were studied extensively and the results are discussed hereafter. The phreatic level at failure - Critical Phreatic Level (CPL), obtained from the experimental analysis was modeled in the software and analyzed. The 28° and 30° slopes for Soil 1 are shown in Figs. 10 and 11 respectively.

Table 4. Parameters of soil

Parameter	Soil 1	Soil 2	Soil 3
Unsaturated unit weight (kN/m^3)	21.1	21.6	21.3
Saturated unit weight (kN/m^3)	22.9	23.3	22.3
Void ratio (e)	0.223	0.205	0.116
Specific gravity (G)	2.63	2.66	2.42
Permeability (k) (m/min)	8.80e^{-4}	3.00e^{-4}	4.36e^{-4}
Stiffness (kN/m^2)	30.0	30.0	30.0
Angle of internal friction (φ)	30.5°	41.3°	28.9°
Unit cohesion (c) (kPa)	24.08	6.26	14.94
Young's modulus (MPa)	40.00	80.00	80.00

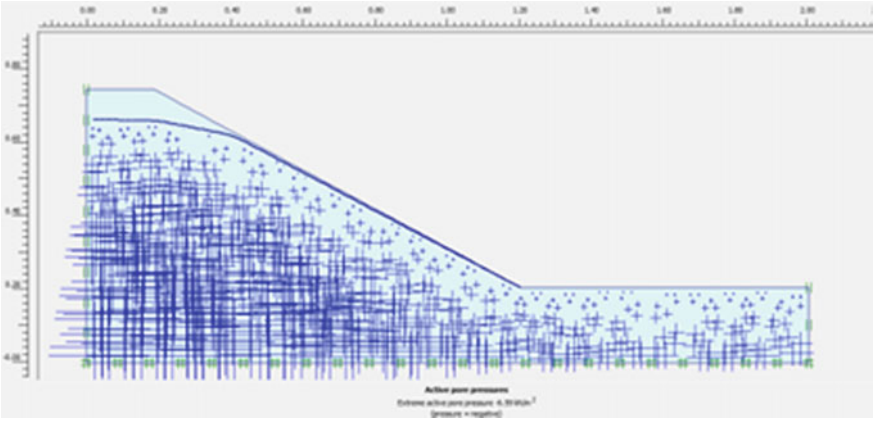

Fig. 10. Critical phreatic level–Soil 1 - 28°

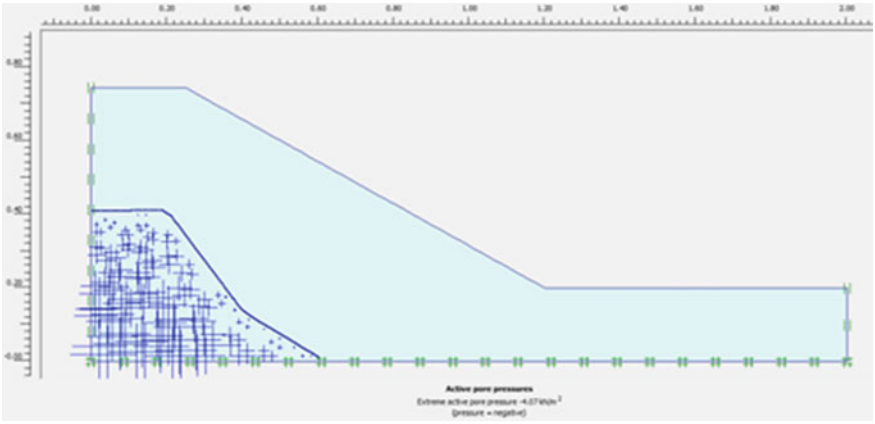

Fig. 11. Critical phreatic level–Soil 2 - 30°

4 Results and Discussion

4.1 Experimental Results

Case 1: Soil 1

Soil - 1 of slope angle 28° with groundwater table

The slope failure occurred after 195 min at a water level of 48 cm from the bottom of the slope. The outflow discharge from the toe region was found to be steady with 1 L per minute after the toe of the slope saturated. The slope had a maximum toe displacement of 0.6 mm. The CPL at failure and slope failure is shown in Figs. 12 and 13.

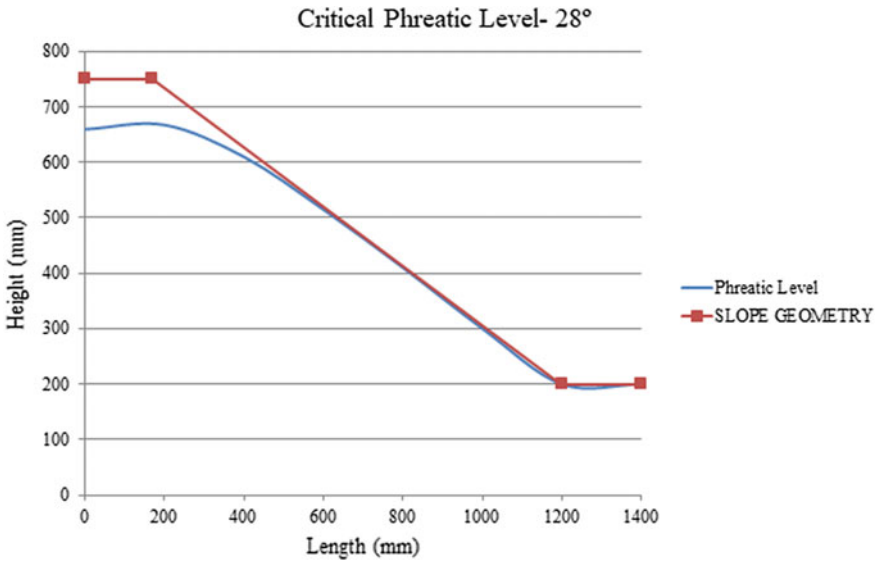

Fig. 12. Critical phreatic level for soil - 1 of slope 28

Fig. 13. Slope failure -28° [soil - 1]

Soil - 1 of slope angle 30° with groundwater table

The slope failure occurred after 160 min at a water level of 46 cm from the bottom of the slope. The outflow discharge from the toe region was found to be steady with 1 L per minute after the toe of the soil slope had saturated. The slope had a maximum toe displacement of 1.02 mm. The CPL at failure and slope failure is shown in Figs. 14 and 15.

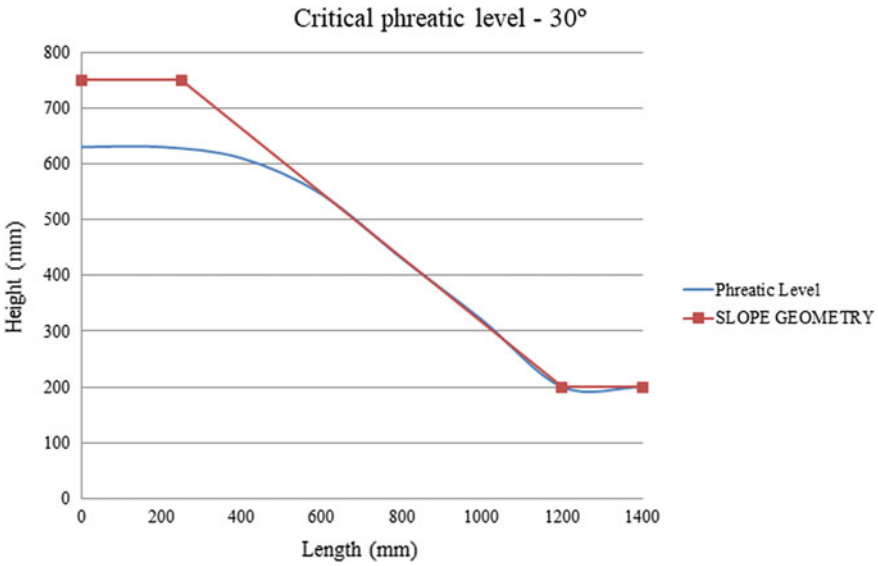

Fig. 14. Critical phreatic level for soil - 1 of slope 30°

Fig. 15. Slope failure - 30° [soil - 1]

Soil - 1 of slope angle 33° with groundwater table

The slope failure occurred after 145 min at a water level of 38.5 cm from the bottom of the slope. The outflow discharge from the toe region was found to be steady with 1.021 L per minute after the toe of the soil slope had saturated. The slope had a maximum toe displacement of 2.15 mm. The CPL at failure and slope failure is shown in Figs. 16 and 17.

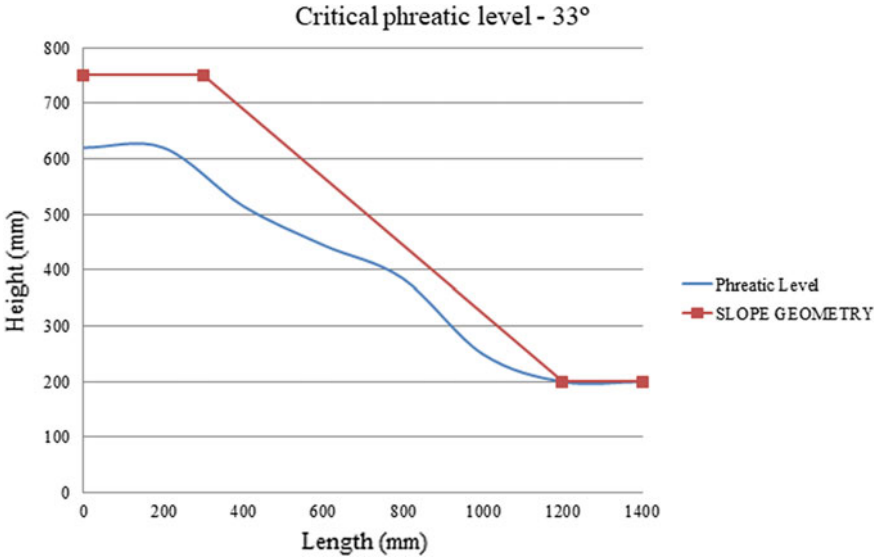

Fig. 16. Critical phreatic level for soil - 1 of slope 33°

Fig. 17. Slope failure - 33° soils - 1

A comparison between different slope angles and their corresponding CPL are shown in Fig. 18 and varying toe displacement is marked against their corresponding slope angles in Fig. 19.

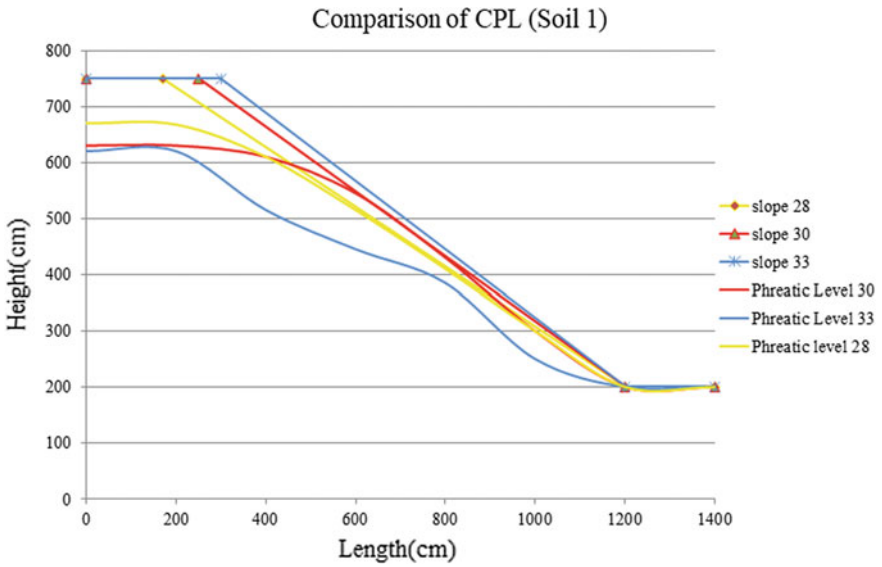

Fig. 18. Different phreatic level for soil - 1

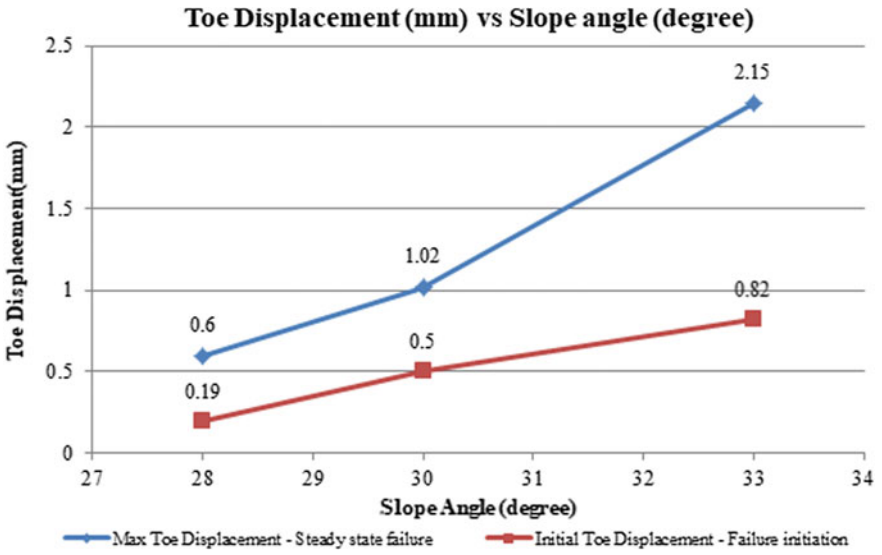

Fig. 19. Toe displacements corresponding to different slope angle

It was observed from the above results that soil with high slope angles fails quicker. CPL for soil with low slope angle was found to be greater than that with steeper slope angles. The soil displacement increased as the slope became steeper.

Case 2: Soil 2

The relatively low permeability and uniform particle size distribution of this soil lead to a considerable capillary rise of water i.e. upward vertical movement of water was faster than the forward horizontal movement. It was observed in this case that the slope failure occurred only when the surface of slope got saturated.

Soil - 2 of slope angle 28° with groundwater table

The failure occurred after 85 min at a water level of 38 cm from the bottom of the slope, recording a face displacement of 4.03 mm. The ultimate failure was observed as soil flow, which occurred after the saturation of the top surface of the slope. The CPL and slope failure is shown in Figs. 20 and 21 respectively.

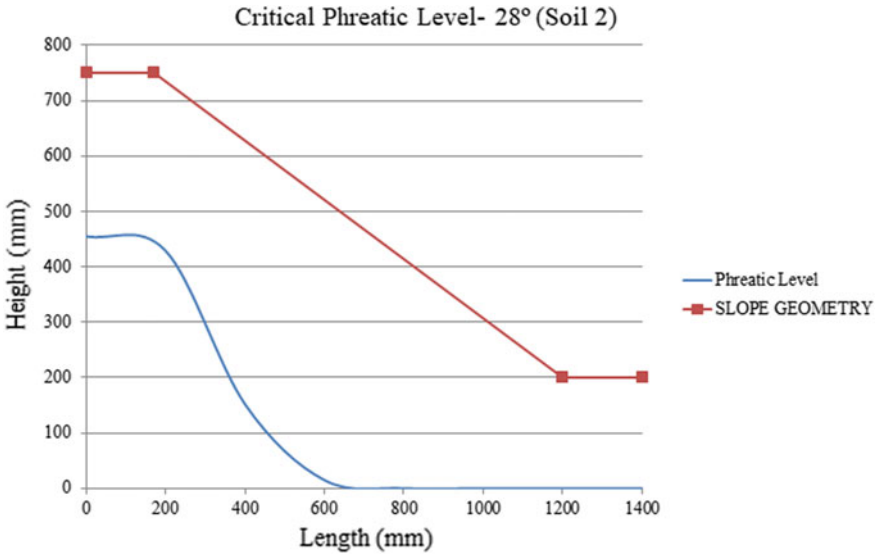

Fig. 20. Critical phreatic level for soil - 2 of slope 28°

Fig. 21. Slope failure - 28° [soil - 2]

Soil - 2 of slope angle 30° with groundwater table

The failure occurred after 75 min at a water level of 38 cm from the bottom of the slope, recording a face displacement of 2.08 mm. The ultimate failure was soil flow which occurred after the saturation of the top surface of the slope and the maximum final face displacement was found to be 5.18 mm. The CPL and slope failure is shown in Figs. 22 and 23 respectively.

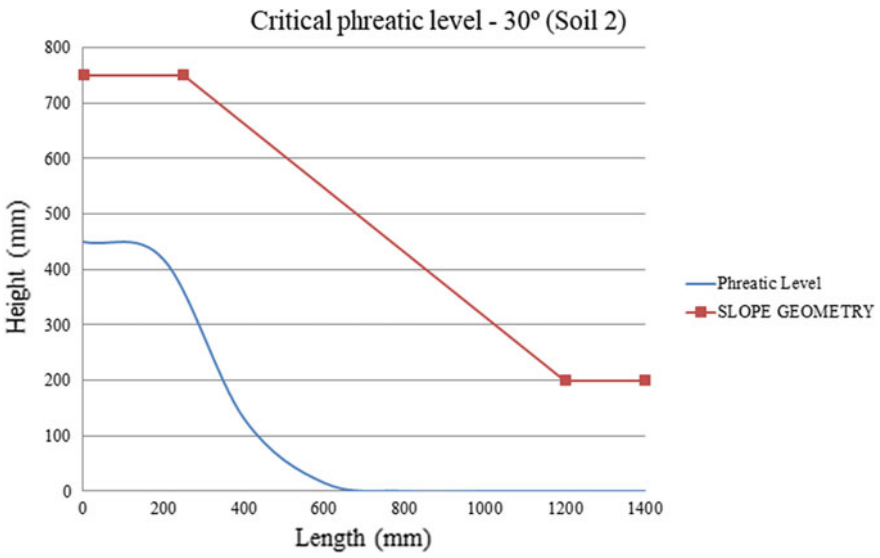

Fig. 22. Critical phreatic level for soil - 2 of slope 30°

Fig. 23. Slope failure - 30° [soil - 2]

As a considerable amount of water moved in the soil slope, there occurred a series of displacements along the face of the soil slope. The ultimate failure occurred when the top of the slope saturated and caused earth flow in both slope geometries.

Case 3: Soil 3

Soil - 3 of slope angle 28° with groundwater table

The failure occurred after 115 min and the water table was found to be at 43.5 cm from the bottom of the slope. The failure of the slope was observed as considerable settlement and face displacement. Displacement at critical failure was recorded to be 22.1 mm of face displacement and maximum final face displacement was found to be 24.31 mm. The CPL and slope failure is shown in Figs. 24 and 25 respectively.

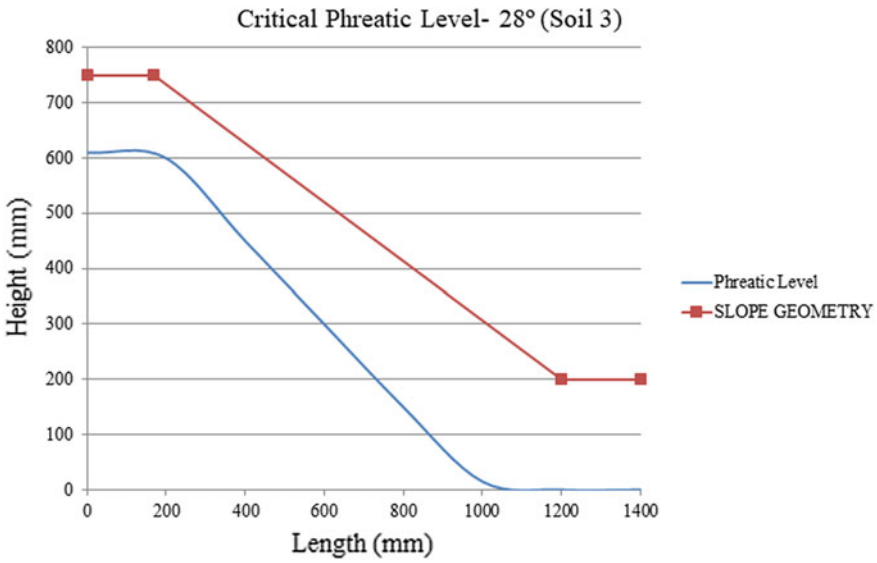

Fig. 24. Critical phreatic level for soil - 3 of slope 28°

Fig. 25. Slope failure - 28° [soil - 3]

Soil - 3 of slope angle 30° with groundwater table

The failure occurred after 110 min and the water table was found to be 44 cm from the bottom of the slope. The major failure of the slope was due to face displacement. Displacement at critical failure was recorded to be 13.39 mm of face displacement and maximum final face displacement was found to be 17.79 mm. The CPL and slope failure is shown in Figs. 26 and 27 respectively.

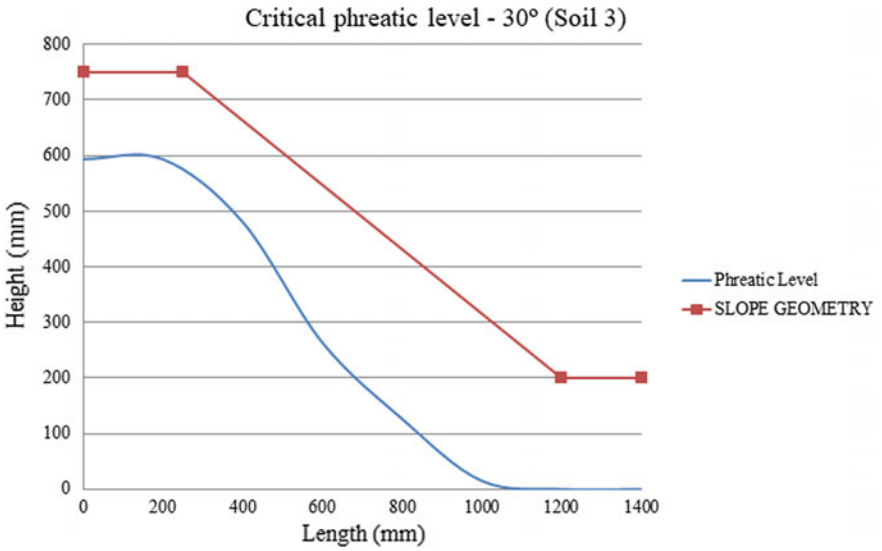

Fig. 26. Critical phreatic level for soil - 3 of slope 30°

Fig. 27. Slope failure - 30° [soil - 3]

Both the slope geometries of Soil - 3 were subjected to high face displacement as the water flowed through the slope. The ultimate failure of the slopes was marked by large displacements and earth movements under the action of water.

4.2 Comparison of CPLs for Different Angles of the Same Soil

By comparing the CPLs for different angles of the same soil, it was evident that the CPL was lower for steeper slopes. The CPLs for different angles and different soils are shown in Figs. 18, 28 and 29. It was observed that steeper slopes have greater displacement and fail quicker than gradual slopes, provided the different slopes are of same density and have same inflow rate of water. CPL for different soils mainly depend on the permeability and particle size distribution of soil (coefficient of curvature and coefficient of uniformity), which in turn increases the seepage pressures and total driving moments generated, reducing the mobilization of maximum shear strength along the slip surfaces. The nature of slope failure also depends on the particle size distribution of the soil.

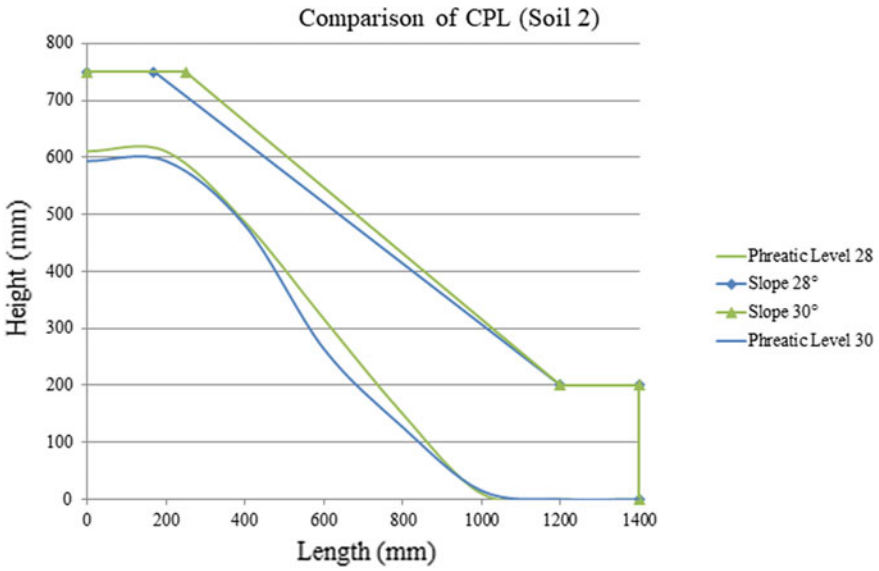

Fig. 28. Different phreatic level for soil - 2

4.3 Comparison of CPLs for Different Soils at Same Slope Angle

The CPLs of different soils varied from each other though they had similar slope geometries. The displacements happened at the toe region or on the slope face, varying from small displacements of 2 mm to much higher displacements of 20 mm. Depending on various characteristics and properties of the soil, the water movement at the specified inflow rate dominated in either vertical upward movement i.e. capillary rise or forward horizontal movement, causing different modes of failure too. The CPLs of different soils of same slope geometries are graphically compared in Figs. 30 and 31.

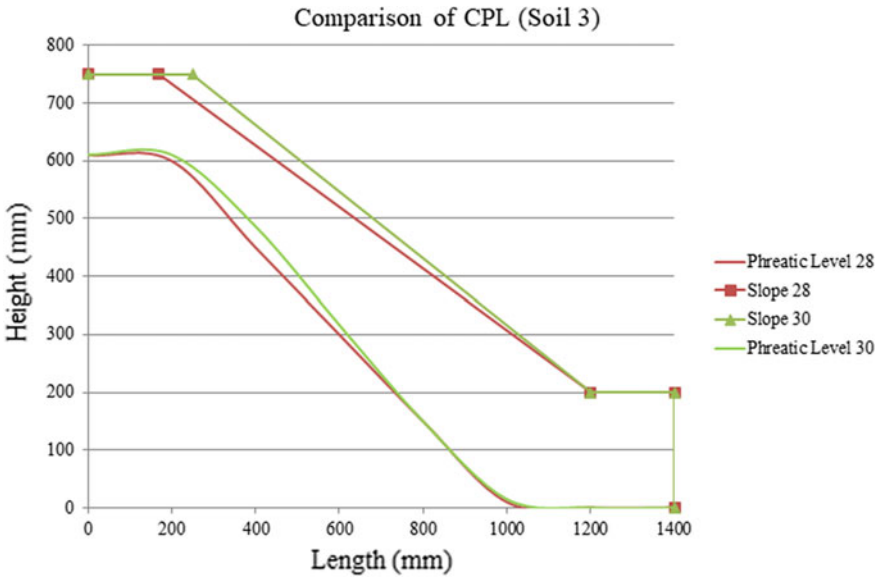

Fig. 29. Different phreatic level for soil - 3

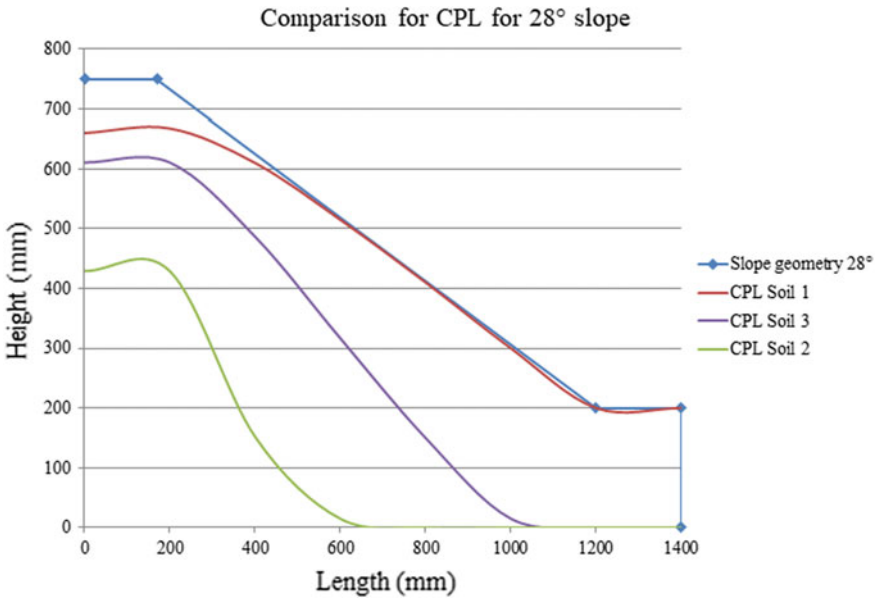

Fig. 30. Critical phreatic levels for slope angle 28°

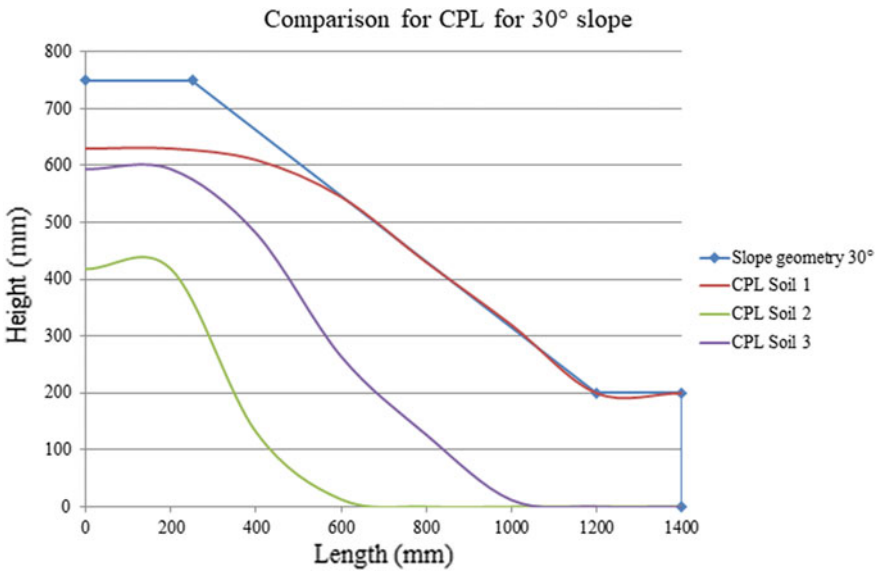

Fig. 31. Critical phreatic levels for slope angle 30°

5 Numerical Results

The experimental results were modeled in PLAXIS and validated. It was found that the failure patterns and displacements observed in the software and the experimental studies were similar. A possible explanation for the minor difference between the experimental and numerical displacement results could be the fact that PLAXIS 2D runs a plastic analysis for the slope geometries until it reaches ultimate failure, incorporating automatic time steps. However, in the experimental studies, the displacement was noted at the time of failure and the tests were run only for a limited duration. The displacement values reported from the numerical analysis are the maximum values attained. However, if the displacements are considered at the location where the displacement was measured in the experimental study, the difference between the two values would be much lesser. The failure patterns for different slope geometries for different types of soils are discussed below.

5.1 Homogenous Soil Slope with Ground Water Table

After the CPLs from the experimental results were simulated in the software, the failure displacement diagrams for 28° and 30° slopes were obtained and are represented in Table 5 and Fig. 32. Slight differences in the total displacements of experimental and numerical models may be due to the difference in the field density achieved in experimental and numerical study. The total displacement diagrams from FEM analysis for different soils at 30º slope angles are shown in Figs. 33, 34 and 35. The failure diagrams and displacement values obtained from FEM analyses for Cases 1 and 2 are similar to the failure patterns observed in the experimental studies, thereby validating

the experimental procedure and the sensor readings for the phreatic levels. From the experimental analysis and the subsequent analytical validation, it was observed that the CPL and the slope failure parameters depended on the soil properties such as soil group classification, coefficient of curvature and uniformity, etc. This analysis can thus be carried forward to obtain a reliable method that uses the aforementioned soil parameters to predict the CPL and slope failure parameters such as the mode of failure, maximum displacement, etc.

Table 5. Displacement (mm) – experimental and numerical results

Total displacement (mm)		
Slope angle	Experimental results	Numerical results
Soil 1		
28°	0.19	0.10
30°	0.50	0.20
Soil 2		
28°	3.69	30.47
30°	2.08	32.31
Soil 3		
28°	22.10	40.59
30°	13.39	40.74

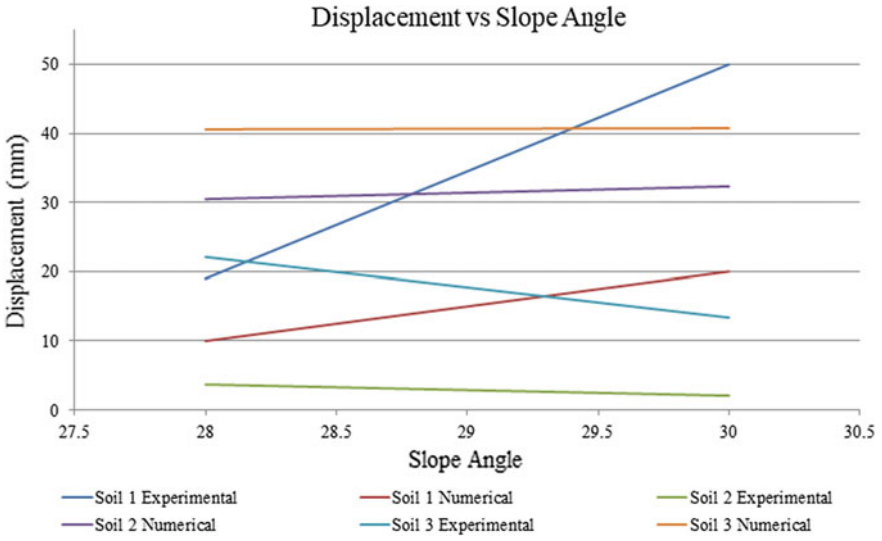

Fig. 32. Displacement vs slope angle for different soil types

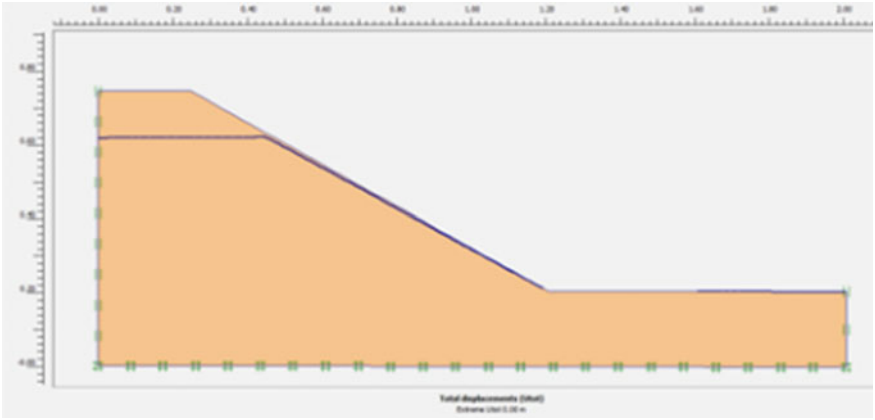

Fig. 33. Soil - 1 total displacement

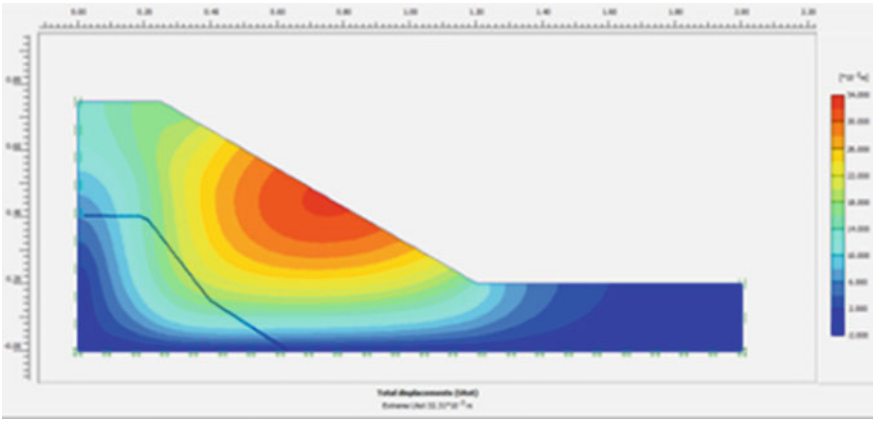

Fig. 34. Soil - 2 total displacements

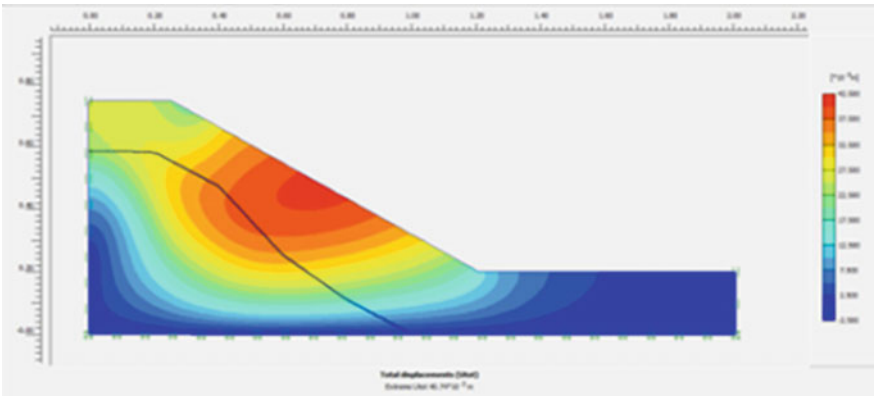

Fig. 35. Soil - 3 total displacements

6 Conclusion

From the experimental data and results, it was observed that sudden ground water fluctuation is one of the predominant reasons for slope failure to occur. The failure of the slope occurred due to both toe saturation and slope saturation. On steeper homogeneous slopes, the CPL was lower and slope failure occurred within a shorter time span of steady state flow, indicating that they are more unstable under the given conditions. The surface displacements were found to be larger in steeper slopes. The slope failure pattern also depended upon the soil characteristics, and showed significant variation in terms of the Coefficient of Uniformity (C_u). Soil 2, for which the C_u is 6.85, the failure was drastic when compared to Soil 1 and Soil 3, which has a C_u of 3.22 and 3.04 respectively. By knowing the Coefficient of Uniformity, C_u and Coefficient of Curvature, C_c of a soil type, an approximate prediction of the CPL and type of slope failure can be done. The failure occurred upon toe saturation in the case of soil slopes with highly plastic soil, whereas for slopes having soil with low plasticity index, the failure took place before the water reached the toe. We can also conclude that plasticity index also has an impact on the type of failure. The values of the toe and surface displacements of the above soil slopes can be compared with similar soil conditions in hilly terrains to provide an empirical relation that predicts mass movements. This can be used as an early warning system by monitoring the initial displacements of soil slope using inclinometers, along with the rate of precipitation or phreatic level rise.

Acknowledgment. We would like to express our gratitude to Amrita School of Engineering, Amrita Vishwa Vidyapeetham, India for providing the necessary funds and facilities required for the successful completion of the project. We express our heartfelt thanks to Mr. K. Sreenivasan and the supporting lab staff for their sincere support.

References

Alamshahi, S., Hataf, N.: Bearing capacity of strip footings on sand slopes reinforced with geogrid and grid-anchor. Geotext. Geomembr. **27**, 217–226 (2009). https://doi.org/10.1016/j.geotexmem.2008.11.011

Aryal, K.: Slope Stability Evaluations by Limit Equilibrium and Finite Element Methods. Doctoral Thesis, Norwegian University of Science and Technology (2006)

Bray, J., Travasarou, T.: Simplified procedure for estimating earthquake-induced deviatoric slope displacements. J. Geotech. Geoenviron. Eng. **133**, 381–392 (2007). https://doi.org/10.1061/(asce)1090-0241(2007)133:4(381)

Butterfield, R., Andrawes, K.: An air activated sand spreader for forming uniform sand beds. Géotechnique **20**, 97–100 (1970). https://doi.org/10.1680/geot.1970.20.1.97

Chen, H., Lee, C.: A dynamic model for rainfall-induced landslides on natural slopes. Geomorphology **51**, 269–288 (2003). https://doi.org/10.1016/s0169-555x(02)00224-6

Crosta, G., Prisco, C.: On slope instability induced by seepage erosion. Can. Geotech. J. **36**, 1056–1073 (1999). https://doi.org/10.1139/cgj-36-6-1056

Dave, T., Dasaka, S.: Assessment of portable traveling pluviator to prepare reconstituted sand specimens. Geomech. Eng. **4**, 79–90 (2012). https://doi.org/10.12989/gae.2012.4.2.079

Drnevich, V., Rad, N., Tumay, M.: Factors affecting sand specimen preparation by raining. Geotech. Test. J. **10**, 31–37 (1987). https://doi.org/10.1520/gtj10136j

Dupla, J., Canou, J., Gouvenot, D.: An advanced experimental set-up for studying a monodirectional grout injection process. Ground Improv. **8**, 91–99 (2004). https://doi.org/10.1680/grim.8.3.91.41117

Gasmo, J., Rahardjo, H., Leong, E.: Infiltration effects on stability of a residual soil slope. Comput. Geotech. **26**, 145–165 (2000). https://doi.org/10.1016/s0266-352x(99)00035-x

Hack, R., Alkema, D., Kruse, G., et al.: Influence of earthquakes on the stability of slopes. Eng. Geol. **91**, 4–15 (2007). https://doi.org/10.1016/j.enggeo.2006.12.016

Hammouri, N., Malkawi, A., Yamin, M.: Stability analysis of slopes using the finite element method and limiting equilibrium approach. Bull. Eng. Geol. Environ. **67**, 471–478 (2008). https://doi.org/10.1007/s10064-008-0156-z

Iverson, R., Reid, M.: Gravity-driven groundwater flow and slope failure potential: 1. Elastic effective-stress model. Water Resour. Res. **28**, 925–938 (1992). https://doi.org/10.1029/91wr02694

Kildalen, S., Stenhamar P.: NGI laboratory sand rainer. Internal report 51505–15, Norwegian Geotechnical Institute (1977)

Kim, J., Jeong, S., Park, S., Sharma, J.: Influence of rainfall-induced wetting on the stability of slopes in weathered soils. Eng. Geol. **75**, 251–262 (2004). https://doi.org/10.1016/j.enggeo.2004.06.017

Kolbuszewski, J.: An experimental study of the maximum and minimum porosities of sands. In: Proceedings of the Second International Conference of Soil Mechanics and Foundation Engineering, vol. 1, pp. 158–165 (1948)

Kolbuszewski, J., Jones, R.: The preparation of sand samples for laboratory testing. Proc. Midl. Soil Mech. Found. Eng. Soc. **4**, 107–123 (1961)

Lam, L., Fredlund, D., Barbour, S.: Transient seepage model for saturated–unsaturated soil systems: a geotechnical engineering approach. Can. Geotech. J. **24**, 565–580 (1987). https://doi.org/10.1139/t87-071

Laouafa, F., Darve, F.: Modelling of slope failure by a material instability mechanism. Comput. Geotech. **29**, 301–325 (2002). https://doi.org/10.1016/s0266-352x(01)00030-1

Ng, C., Pang, Y.: Influence of stress state on soil-water characteristics and slope stability. J. Geotech. Geoenviron. Eng. **126**, 157–166 (2000). https://doi.org/10.1061/(asce)1090-0241(2000)126:2(157)

Ng, C., Shi, Q.: A numerical investigation of the stability of unsaturated soil slopes subjected to transient seepage. Comput. Geotech. **22**, 1–28 (1998). https://doi.org/10.1016/s0266-352x(97)00036-0

Pradel, D., Raad, G.: Effect of permeability on surficial stability of homogeneous slopes. J. Geotech. Eng. **119**, 315–332 (1993). https://doi.org/10.1061/(asce)0733-9410(1993)119:2(315)

Rahardjo, H., Lee, T., Leong, E., Rezaur, R.: Response of a residual soil slope to rainfall. Can. Geotech. J. **42**, 340–351 (2005). https://doi.org/10.1139/t04-101

Rahimi, A., Rahardjo, H., Leong, E.: Effect of antecedent rainfall patterns on rainfall-induced slope failure. J. Geotech. Geoenviron. Eng. **137**, 483–491 (2011). https://doi.org/10.1061/(asce)gt.1943-5606.0000451

Ramkrishnan, R., Karthik, V., Unnithan, M.S., Kiran Balaji, R., Athul Vinu, M., Venugopalan, A.: Stabilization of seepage induced soil mass movements using sand drains. Geotech. Eng. J. SEAGS & AGSSEA, **48**(4), 129–137 (2017)

Rinaldi, M., Casagli, N., Dapporto, S., Gargini, A.: Monitoring and modelling of pore water pressure changes and riverbank stability during flow events. Earth Surf. Proc. Land. **29**, 237–254 (2004). https://doi.org/10.1002/esp.1042

Saussus, D., Frost, J.: Simulating the membrane contact patterns of triaxial sand specimens. Int. J. Numer. Anal. Meth. Geomech. **24**, 931–946 (2000). https://doi.org/10.1002/1096-9853(200010)24:12<931:aid-nag100>3.0.co;2-4

Saygili, G., Rathje, E.: Empirical predictive models for earthquake-induced sliding displacements of slopes. J. Geotech. Geoenviron. Eng. **134**, 790–803 (2008). https://doi.org/10.1061/(asce)1090-0241(2008)134:6(790)

Sazzad, M., Haque, M.: Effect of surcharge on the stability of slope in a homogeneous soil by FEM. In: 2nd International Conference on Advances in Civil Engineering, pp 315–318 (2014)

Simon, A., Larsen, M., Hupp, C.: The role of soil processes in determining mechanisms of slope failure and hillslope development in a humid-tropical forest eastern Puerto Rico. Geomorphology **3**, 263–286 (1990). https://doi.org/10.1016/0169-555x(90)90007-d

Smethurst, J., Clarke, D., Powrie, W.: Seasonal changes in pore water pressure in a grass-covered cut slope in London Clay. Géotechnique **56**, 523–537 (2006). https://doi.org/10.1680/geot.2006.56.8.523

Vaid, Y.: Relative density of pluviated sand samples. Jpn. Soc. Soil Mech. Found. Eng. **24**(2), 101–105 (1984)

Vaid, Y., Negussey, D.: Relative density of pluviated sand samples. Soils Found. **24**, 101–105 (1984). https://doi.org/10.3208/sandf1972.24.2_101

Vaid, Y., Negussey, D.: Preparation of reconstituted sand specimens. Advanced triaxial testing of soils and rock, ASTM STP977. In: Donaghe, R.T., Chaney, R.C., Silver, M.L., (eds) ASTM International, West Conshohocken, PA, pp. 405–417 (1988)

Vandamme, J., Zou, Q.: Investigation of slope instability induced by seepage and erosion by a particle method. Comput. Geotech. **48**, 9–20 (2013). https://doi.org/10.1016/j.compgeo.2012.09.009

Vanmarcke, E.: Probabilistic modeling of soil profiles. J. Geotech. Eng. Div. **103**(11), 1227–1246 (1977)

Viggiani, G., Tamagnini, C.: Ground movements around excavations in granular soils: a few remarks on the influence of the constitutive assumptions on FE predictions. Mech. Cohesive-frictional Mater. **5**, 399–423 (2000). https://doi.org/10.1002/1099-1484(200007)5:5<399:aid-cfm101>3.0.co;2-r

Wang, J., Wang, C., Lu, G.: Application of PLAXIS to simulation of foundation excavation and support. Chin. J. Rock Mech. Eng. **35** (2007)

Wilson, R., Keefer, D.: Dynamic analysis of a slope failure from the 6 August 1979 Coyote Lake, California, earthquake. Int. J. Rock Mech. Min. Sci. Geomech. Abstr. **21**, 220–221 (1984). https://doi.org/10.1016/0148-9062(84)90499-6

Zhao, Y., Gafar, K., Elshafie, M., Deeks, A., Knappett, J., Madabushi, S.: Calibration and use of new automatic sand pourer. In: Sixth International Conference on Physical Modeling in Geotechnics, Hong Kong, 4–6 August, Taylor & Francis, London, pp. 265–270 (2006)

Zhu, H., Shi, B., Zhang, J., et al.: Distributed fiber optic monitoring and stability analysis of a model slope under surcharge loading. J. Mt. Sci. **11**, 979–989 (2014). https://doi.org/10.1007/s11629-013-2816-0